THE JOURNAL OF PHYSICAL CHEMISTRY C

Article

pubs.acs.org/JPCC

Substrate Effect on the Refractive Index Sensitivity of Silver Nanoparticles

Erik Martinsson,[†] Marinus A. Otte,[‡] Mohammad Mehdi Shahjamali,[§] Borja Sepulveda,[‡] and Daniel Aili*[,†]

[†]Division of Molecular Physics, Department of Physics, Chemistry and Biology (IFM), Linköping University, SE-581 83 Linköping, Sweden

[‡]Institut Catala de Nanociencia i Nanotecnologia (ICN2), Consejo Superior de Investigaciones Cientificas (CSIC) & CIBER-BBN, Campus UAB, Bellaterra, 08193 Barcelona, Spain

[§]Department of Chemistry, Materials Science & Engineering and International Institute for Nanotechnology, Northwestern University, 2145 Sheridan Road, Evanston, Illinois 60208-3113, United States

Supporting Information

ABSTRACT: The bulk refractive index (RI) sensitivity of dispersed and immobilized silver nanoparticles of three different shapes (spheres, cubes, and plates) is investigated. We demonstrate, both experimentally and theoretically, that the influence of immobilization on the RI sensitivity is highly dependent on the shape of the nanoparticles. A strong correlation is seen between the fraction of the particle surface area in direct contact with the substrate and the decrease in RI sensitivity when the particles are immobilized on a glass substrate. The largest decrease (−36%) is seen for the most sensitive nanoparticles (plates), drastically reducing their advantage over other nanoparticle shapes. The shape-dependent substrate effect is thus an important factor to consider when designing nanoplasmonic sensors based on colloidal noble-metal nanoparticles.

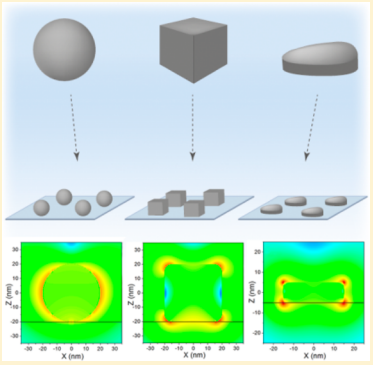

Noble-metal nanoparticles have become attractive signal transducers in optical biosensors because of their ability to respond to small changes in the refractive index (RI) in close vicinity to the nanoparticles.[1−5] This property originates from the excitation of free surface electrons in metal nanostructures, a phenomenon known as localized surface plasmon resonance (LSPR), where the resonance frequency of the electrons is highly dependent on the dielectric environment.[6,7] By varying the size, shape, and composition of the metal nanoparticles, their resonance frequency can be tuned over the entire visible spectrum, creating plasmonic particles with unique optical properties showing different sensitivities for detecting RI changes in their close proximity.[8−10] The advancement in methods for chemical synthesis of nanomaterials during the last decades now enables the production of defined and uniform nanostructures with respect to geometrical, physical, and chemical properties.[11−13] Combined with the progress in nanofabrication and a better theoretical understanding of plasmonics, this has led to an increasing interest in LSPR-based sensors as they pose an attractive alternative to the conventional surface plasmon resonance (SPR) technique for sensing applications.[14−16]

Although most nanoparticles are produced by wet chemistry methods, resulting in particles suspended in aqueous buffer, it is for practical reasons beneficial to immobilize the nanoparticles on a solid support to realize a nanoplasmonic sensing device.[17,18] Suspensions of nanoparticles are not thermodynamically stable, and both specific or unspecific binding of analytes or other molecules in the sample as well as changes in pH, ionic strength, and temperature may cause the particles to aggregate, resulting in a dramatic optical response that would overshadow any optical shift caused by RI changes.[19,20] Tethering the nanoparticles to a substrate effectively prevents nanoparticle aggregation and facilitates nanoparticle functionalization and also enables ligand regeneration (removal of the analyte) and integration with microfluidic systems. Several surface chemistry protocols have been developed for immobilization of metal nanoparticles on solid supports including both covalent and electrostatic binding strategies.[21−23] However, nanoparticle immobilization can have a profound effect on the electromagnetic (EM) field distribution and field intensity around the particles, shifting a large part of the near-field EM into the substrate, which changes the polarizability of the free electrons in the particles and hence affects their RI sensitivity.[24−27] Studies on nanostructures fabricated by lithography have shown that the substrate has a large impact on the sensitivity and that the effect can be minimized by suspending nanostructures on pillars[28,29] or by decreasing the RI of the substrate.[30] Interactions with the substrate can also lead to plasmon-mode hybridization generating higher plasmonic modes with various RI sensitivities.[31−33] Although particle−surface interactions have been

Received: August 20, 2014
Published: October 7, 2014

   dx.doi.org/10.1021/jp5084086 | J. Phys. Chem. C 2014, 118, 24680−24687

extensively studied both experimentally and theoretically, there are few reports on how the substrate influences the RI sensitivity in nanoplasmonic sensors based on immobilized colloidal metal nanoparticles.

In the present work, we have compared the bulk RI sensitivity (η_B) for dispersed and surface-immobilized silver nanoparticles of three different shapes (nanospheres, nanocubes, and nanoplates) both experimentally by spectroscopic measurements and theoretically using finite-difference time-domain (FDTD) calculations. The results show a strong correlation between the fraction of the particle surface in contact with the substrate and the decrease in the RI sensitivity upon immobilization. Particles exhibiting high bulk RI sensitivity in solution can hence lose a significant part of their sensitivity when attached to a solid support depending on their geometrical shape and redistribution of the near-field EM upon immobilization. Minimizing surface effects is thus a highly important aspect to consider when developing refractometric nanoplasmonic sensors, especially as a significant amount of work is dedicated to synthesis of new elaborate plasmonic nanoparticles with improved RI sensitivities.

EXPERIMENTAL DETAILS

Nanoparticle Synthesis. *Silver Nanospheres.* Spherical silver colloids (40 nm in diameter) were purchased from BBI solutions (U.K.).

Silver Nanocubes. In a standard synthesis, 5 mL of ethylene glycol (EG) was added to a 100 mL round-bottomed flask and heated while stirring in an oil bath at 150 °C. After the temperature had reached 150 °C, 0.06 mL of NaSH (3 mM in EG) was quickly injected into the heated solution. Five minutes later, 0.5 mL of HCl solution (3 mM) was injected into the heated reaction solution, followed by the addition of 1.5 mL of poly(vinyl pyrrolidone) (PVP, MW = 55 000, 20 mg/mL in EG). 0.4 mL of silver trifluoroacetate (282 mM in EG) was added to the mixture. After the addition of CF_3COOAg, the transparent reaction solution became yellowish in 1 min, indicating the formation of silver seeds. The reaction was allowed to proceed for different periods of time before it was quenched by ice-water bath. The particles were collected by centrifugation and washed with ethanol once., then DI water two times to remove excess PVP. It is good to note that during the entire process the flask was capped with a glass stopper except during the addition of reagents.

Silver Nanoplates. Triangular silver nanoprisms (SNPs) preparation was carried out by using a modified protocol based on previous reports. In a typical synthesis, ultrapure water (95 mL), $AgNO_3$ (0.6 mL, 30 mM), and sodium citrate (1 mL, 35 mM) were combined in a 250 mL three-necked flask. The flask was immersed in an ice bath, and the solution was bubbled with nitrogen gas under vigorous stirring for 1 h. Then, 0.5 mL of aqueous solution of $NaBH_4$ (70 mM, freshly prepared with ice-cold ultrapure water prior to injection) was rapidly injected into the solution. Over the next 20 min, 5−10 drops of $NaBH_4$ solution were added to the reaction solution at 2 min intervals. Then 0.5 mL solution of BSPP (5 mM) and 0.5 mL of solution of $NaBH_4$ were simultaneously added dropwise to the solution over a 10 min period. The resulting colloid of Ag nanoparticles was gently stirred for 3 h in the ice bath and allowed to age at ∼4 °C for 24 h in a dark place. For the photomediated growth of SNPs, typically, 30 mL colloid solution of the prepared silver nanoparticles was irradiated by a 150 W halogen lamp coupled to an optical bandpass filter centered at 550 ± 20 nm for 2−5 h. The prepared SNP batch was allowed to truncate through aging (∼12 months), creating truncated prisms and circular nanodiscs.

Surface Preparation with APTES. Borosilicate glass microscope slides (Fisher Scientific) were cut into 9 mm × 20 mm pieces using a glass cutter. Prior to silanization the surfaces were cleaned in a solution containing a 5:1:1 mixture by volume of Milli-Q water, 30% hydrogen peroxide (Merck KGaA), and 25% ammonia (Merck KGaA) for at least 20 min at 85 °C and thoroughly rinsed with Milli-Q water. Cleaned glass substrates were placed in a chamber containing 200 μL of 3-aminopropyltriethoxysilane (Sigma-Aldrich), and the temperature was increased to 60 °C at 6 mbar pressure for 10 min before it was increased to 150 °C for 1 h. The surfaces were rinsed by ultrasonication in xylene (VWR) for 15 s, rinsed, and stored in xylene until use (within 1 week). Prior to use, the substrates were dried at 120 °C for 1 h and allowed to cool to room temperature. 200 μL of prepared nanoparticle solution was added to the substrates and incubated for 1 h, followed by rinsing with Milli-Q water.

Surface Preparation with Polyelectrolytes. Polyelectrolyte (PE) solutions of polyethylenimine (PEI, MW ≈ 750 000, Sigma-Aldrich), polystyrene sulfonate (PSS, MW ≈ 75 000, Sigma-Aldrich), and poly(allylamine hydrochloride) (PAH, MW ≈ 56 000, Sigma-Aldrich) were prepared with a concentration of 2 mg/mL in 0.5 M NaCl (Sigma-Aldrich) aqueous solutions. Glass slides (9 mm × 20 mm) were prepared and cleaned using the same procedure as prior to silanization. First, 200 μL of PEI was added to the surfaces for 15 min, followed by rinsing with Milli-Q water. Different PE thicknesses were produced by incubating the surfaces with 200 μL of PSS and PAH for 15 min, followed by rinsing with Milli-Q creating surfaces with 5, 9, 13, or 17 PE layers. PAH is a positively charged PE and was always the topmost layer, which enabled immobilization of citrate-stabilized silver nanoparticles by means of electrostatic interactions. 200 μL of the prepared nanoparticle suspensions was applied on the substrates and incubated for 1 h, followed by rinsing with Milli-Q water.

Refractive Index Sensitivity Measurements. Bulk RI sensitivity measurements were performed using sucrose−water mixtures with varying sucrose (Merck KGaA) concentrations from 0 to 50% in steps of 10% ranging from n = 1.33 to 1.42 in RI, determined using an Abbe refractometer. The RI sensitivity for nanoparticles in solution was determined by centrifuging 50 μL of the prepared particle solutions at 12 000 rpm for 10 min, removing the supernatant, and redispersing the particles in the sucrose−water mixtures. The RI sensitivity of nanoparticles attached to glass surfaces functionalized either by APTES or by PE layers was determined by submerging the substrates in a cuvette filled with the different sucrose−water mixtures. Extinction spectra were collected using a Shimadzu UV-2450 spectrophotometer with 0.1 nm resolution. The RI sensitivity was determined by linear regression of the plasmon peak maxima plotted as a function of the RI.

FDTD Simulations. Scattering spectra and the near-field EM profiles were numerically calculated using the FDTD formalism, employing the commercially available Lumerical Software Package. Nanostructures were modeled as either single Ag spherical (D = 40 nm), disk-shaped (H = 10 nm, D = 30 nm), or cubic (L = 40) geometries, which, if necessary, were located on top of a rectangular substrate (n = 1.52). The nanocubes were modeled with rounded corners with radii of 5 nm. For all nanostructures, optical constants for silver were

dx.doi.org/10.1021/jp5084086 | J. Phys. Chem. C 2014, 118, 24680−24687

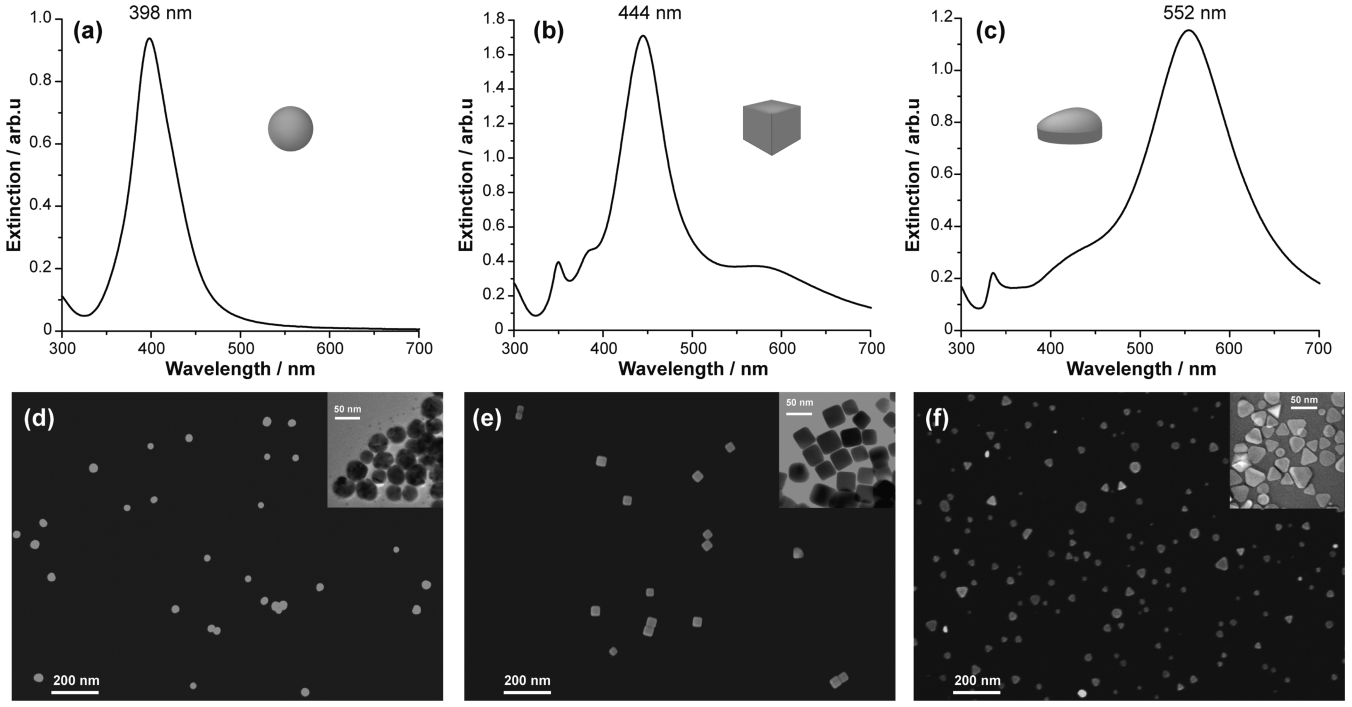

Figure 1. Extinction spectra and SEM+TEM (inset) images of silver nanospheres (a,d), nanocubes (b,e), and nanoplates (c,f).

Table 1. Experimental and Theoretical Data of the Physical Properties and Refractive Index Sensitivities of Dispersed and Immobilized Silver Nanoparticles of Different Shapes

		experimental data				theoretical calculations				
shape	solution or substrate	λ_{max} (nm)	η_B (nm/RIU)	FOM	$\Delta\eta_B$ (%)	λ_{max} (nm)	η_B (nm/RIU)	FOM	$\Delta\eta_B$ (%)	X_A (%)
nanospheres	solution	398	144 ± 4	3.0		407	148	3.3		
	substrate	402	140 ± 5	2.9	−3	410	137	3.0	−7	5[a]
nanocubes	solution	444	158 ± 2	3.3		458	204	3.7		
	substrate	448	124 ± 2	2.5	−21	469	146	2.6	−28	17
nanoplates	solution	552	315 ± 6	3.6		489	233	4.4		
	substrate	558	200 ± 5	2.1	−36	508	133	2.7	−43	30[b]

[a]Estimated value. [b]Calculated for a circular nanodisc.

used.[34] The total simulation volume was equal to 1 μm^3. For the scattering spectra, a simulation grid size of 0.5 nm was used, while for the near-field EM profiles a finer resolution of 0.25 nm was employed. To assess the bulk sensing performance of the nanostructures, the RI of the dielectric environment surrounding the nanostructures was varied between n = 1.33 and 1.43, and the value of slope of the linear fit through the obtained values of λ_{LSPR} was used as an indication of the bulk RI sensitivity.

RESULTS AND DISCUSSION

Silver nanospheres (average diameter: 33 nm) were purchased from BBI Solutions (U.K.), while the nanocubes and nanoplates were chemically synthesized in the lab. Nanocubes with an average length of 35 nm were produced using a previously reported synthesis protocol using PVP as stabilization agent.[35] The nanoplates were created by first synthesizing a batch of SNPs using a photomediated synthesis protocol,[36,37] which was allowed to oxidize into highly truncated prisms. Truncated prisms or circular nanodiscs were preferred over well-defined triangular SNPs because the spontaneous oxidation/truncation of prisms would interfere with the RI sensitivity measurements. The silver nanoplates used in the study had an average size of 30 nm and a thickness of 5−10 nm.

Extinction spectra (acquired in water) of the silver nanoparticles used in this study are shown in Figure 1a−c with the position of their respective plasmon peak indicated. One major plasmon band originating from dipolar excitation can be seen for each particle type at 398, 444, and 552 nm for nanospheres, nanocubes, and nanoplates, respectively. Inspection of the samples using transmission electron microscopy (TEM) (Figure 1d−f, inset) revealed that the sample with nanoplates exhibited a relatively large size distribution caused by various degrees of truncation or rounding, which also gives rise to a rather broad plasmon peak. The samples containing nanospheres and nanocubes showed a high monodispersity with a small size variation and hence narrow plasmon bands.

All particles have a net-negative surface charge, which enables an electrostatic immobilization to positively charged surfaces. We functionalized glass surfaces with 3-aminopropoyltriethoxysilane (APTES) for immobilization of the nanoparticles. A well-ordered monolayer of APTES is critical to obtain a homogeneous surface distribution of particles and to avoid particle aggregation, which gives rise to unwanted coupled plasmon modes. Vapor deposition of APTES followed by

dx.doi.org/10.1021/jp5084086 | J. Phys. Chem. C 2014, 118, 24680−24687

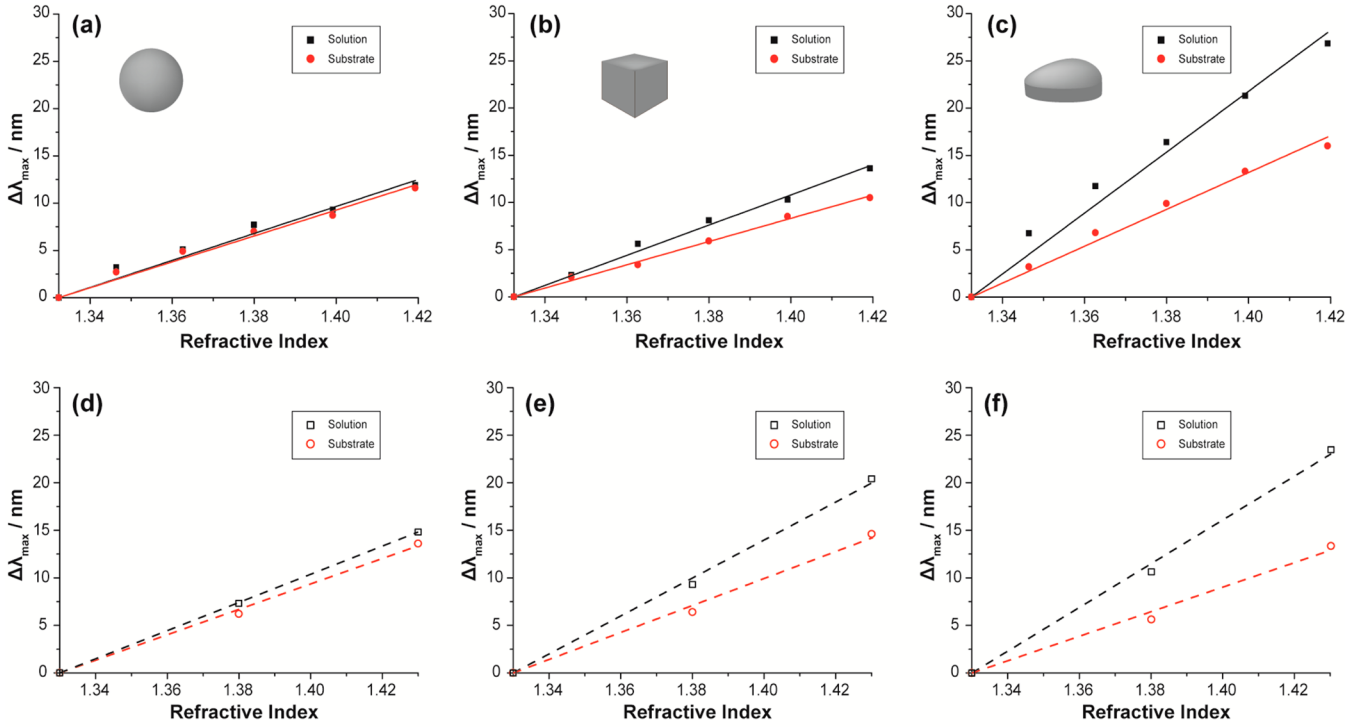

Figure 2. Refractive index sensitivity plots obtained experimentally (a–c) and by FDTD calculations (d–f) for silver nanospheres (a,d), nanocubes (b,e), and nanoplates (c,f) in solution and immobilized on a glass substrate.

extensive rinsing in xylene and curing at 120 °C for 1 h resulted in surfaces suitable for particle immobilization. Surfaces with a relatively low coverage of nanoparticles (<2%) were prepared to avoid plasmonic coupling effects (Figure 1d–f) but high enough for all surfaces to obtain adequate intensities in spectroscopic measurements showing well-defined plasmon bands.

The bulk RI sensitivities were determined using sucrose–water mixtures at various concentrations (0–50%), generating solutions with RI spanning from n = 1.33 to 1.42, which is a standard procedure for determining the sensitivity in refractometric sensing systems. The sensitivity was obtained by plotting the plasmon peak position against the RI of the sucrose–water solutions, where the sensitivity η_B (nm/RIU) is defined as the slope of a linear fit. Dispersed particles were centrifuged and redispersed in the sucrose–water mixtures for determination of the RI sensitivity, while glass substrates having immobilized nanoparticles were completely submerged in the sucrose–water mixtures.

Figure 2a–c shows RI sensitivity plots obtained for both dispersed and immobilized nanoparticles. Nanospheres (Figure 2a) showed essentially no reduction in the RI sensitivity upon immobilization, while the sensitivity for nanocubes (Figure 2b) and nanoplates (Figure 2c) showed a significant decrease in sensitivity. Table 1 summarizes the RI sensitivity data obtained for the three different nanoparticle types. Silver nanospheres showed an average bulk RI sensitivity of 144 nm/RIU in solution, a value that was reduced by only 3% to 140 nm/RIU upon immobilization. For the nanocubes and nanoplates the reduction was 21 and 36%, respectively, from 158 to 124 nm/RIU for nanocubes and from 315 to 200 nm/RIU for nanoplates. Hence, the difference in RI sensitivity between the three types of nanoparticles becomes significantly smaller when they are immobilized to a solid support compared with when the particles are dispersed. Notably, nanocubes show a lower sensitivity than nanospheres after immobilization, while the nanoplates still have the highest sensitivity, although significantly reduced. Also, as a consequence, particle immobilization results in a lower figure of merit (FOM) value for all particles because FOM = η_B/fwhm, where fwhm is the full width at half-maximum of the plasmon resonance peak.[38] The FOM value decreases significantly for the nanocubes and nanoplates as a consequence of the decrease in bulk RI sensitivity combined with a small increase in fwhm.

To verify the experimental results, we performed FDTD calculations of the RI sensitivity for the different nanoparticles. The silver nanostructures were modeled as having spherical (D = 40 nm), cubic (L = 40 nm), or disk-shaped (H = 10 nm, D = 30 nm) geometries. On the basis of TEM data, the nanocubes were modeled with rounded corners with 5 nm radii. RI sensitivity plots obtained from the FDTD calculations are presented in Figure 2d–f. Experimental results agree well with the simulations showing similar appearance of the RI sensitivity plots. Data obtained from the FDTD calculations are summarized in Table 1. The position of the plasmon peak maxima red-shifted a few nanometers for all particles when attached to a solid support, but the experimentally obtained red shifts were smaller than the values obtained through FDTD simulations, except for the nanospheres. The calculated RI sensitivity for nanospheres in solution was 148 nm/RIU, which is in almost perfect agreement with the experimentally obtained value (144 nm/RIU), while the simulations indicate a higher sensitivity for the nanocubes than experimentally verified (204 vs 158 nm/RIU). The nanoplates showed a considerably lower theoretical value compared with the experimental data (315 vs 233 nm/RIU). This deviation can be explained by the polydispersity of the sample, which contained a significant portion of truncated nanoprisms with sharper corners that

dx.doi.org/10.1021/jp5084086 | J. Phys. Chem. C 2014, 118, 24680–24687

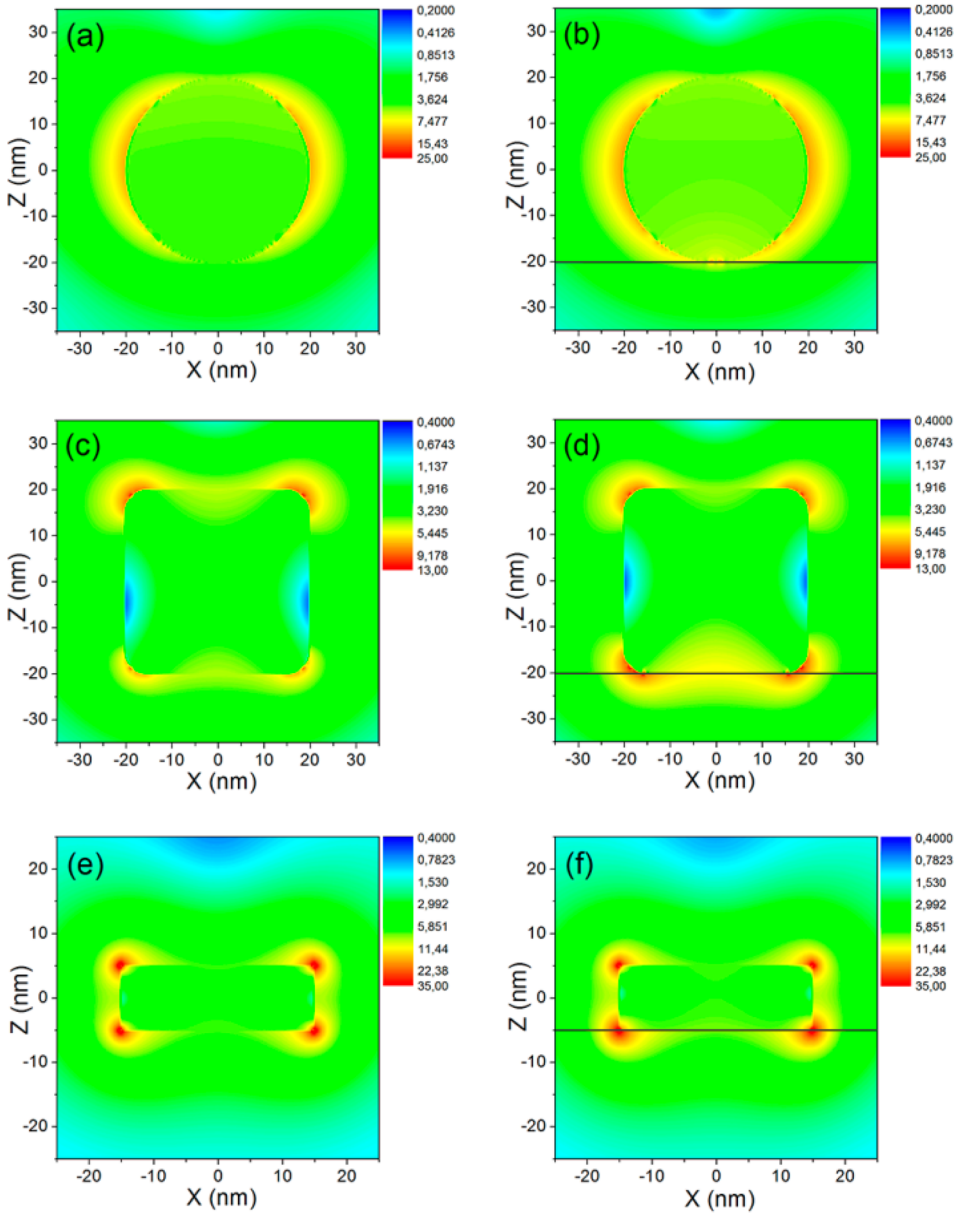

Figure 3. Near-field EM distribution profiles of silver nanospheres (a,b), nanocubes (c,d), and nanoplates (e,f) totally surrounded by a homogeneous dielectric medium (n = 1.33) in panels a, c, and e and immobilized on a solid support (n = 1.52) in panels b, d, and f.

would give rise to a higher RI sensitivity, whereas in the simulations the nanoparticles were assumed to be round nanodiscs. The theoretically calculated decrease in RI sensitivity upon immobilization to a solid support was 7, 28, and 43%, for nanospheres, nanocubes, and nanoplates, respectively, which are slightly higher values compared with experimentally obtained data, 3, 21, and 36%. The differences are, however, small, and simulations and experiments show the exact same trend.

When introducing a substrate with a high RI close to the nanoparticles it is not surprising that the ability to detect RI changes in the external media decreases and that this effect is associated with the particle area connected to the underlying substrate. We calculated the fraction of the total surface area of each particle type that was in direct contact with the substrate when immobilized (X_A) and compared it with the reduction in RI sensitivity (Table 1). As expected, there is an unambiguous correlation between the decrease in RI sensitivity and the fraction of the surface area in contact with the substrate. A flat structure like the nanoplates hence shows the largest decrease in RI sensitivity as compared with nanoparticles with other geometries.

To further understand the substrate influence on the RI sensitivity, we calculated the near-field EM distribution using FDTD simulations for individual nanoparticles in a homogeneous dielectric medium (n = 1.33) and particles immobilized on borosilicate glass (n = 1.52). Figure 3 shows the near-field EM distribution simulations for silver spheres, cubes, and plates at their respective plasmon resonance with the incoming light propagating perpendicular to the substrate and with polarization parallel to the substrate. The simulations show that the near-field EM around the particles changes when they are immobilized on a substrate, redistributing parts of the near-field EM into the substrate, which has a higher RI then the surrounding media. The effect is most pronounced for the nanocubes and the nanoplates where the near-field EM is

dx.doi.org/10.1021/jp5084086 | J. Phys. Chem. C 2014, 118, 24680−24687

concentrated to the edges of the nanoparticles. However, to explain the substrate influence on the RI sensitivity it is more interesting to look at the fraction of the total near-field EM associated with the substrate rather than the relativity small near-field EM redistributions. The near-field EM around a spherical nanoparticle has only a small fraction of the near-field EM inside the substrate. The influence of the substrate on the RI sensitivity is thus small and can almost be neglected for spherical nanoparticles. For a nanocube the near-field EM is most intense at the corners and because four of the corners are facing the substrate a large part of the near-field EM is not accessible for detecting RI changes in the solution. This effect is even more pronounced for a flat structure, like a nanoplate (here calculated as a circular nanodisc), where an even larger fraction of the near-field EM is associated with the substrate. The small redistribution of the near-field EM upon immobilization, showing slightly higher intensities at the sides and corners facing the substrate, explains why the RI sensitivity reduction is higher than the value expected when only considering the geometrical factors and the fraction of the particle surface area in contact with the substrate.

Because there is an obvious correlation between the reduction in the RI sensitivity and the area of the particle in contact with the substrate, this indicates that the reduction can be estimated using the effective medium approximation where the effective dielectric function ($\varepsilon_{\mathrm{eff}}$) can be calculated using the equation

$$\varepsilon_{\mathrm{eff}} = X_{\mathrm{A}}\varepsilon_{\mathrm{sub}} + (1 - X_{\mathrm{A}})\varepsilon_{\mathrm{solv}} \quad (1)$$

where X_{A} is the fractional particle area in direct contact with the substrate. To verify if the effective medium approximation is in fact a suitable model for prediction of the drop in the RI sensitivity, we compared it with FDTD calculations (Figure 4).

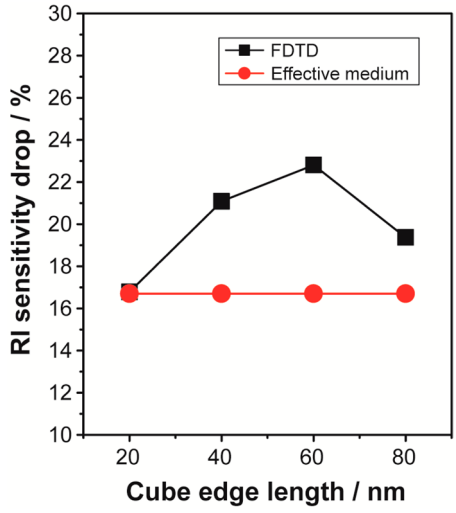

Figure 4. RI sensitivity drop for nanocubes with different side length upon a substrate immobilization calculated with FDTD simulations and by the effective medium approximation.

Nanocubes with various sizes were used for the comparison, and because the fractional particle area in contact with the substrate is constant for nanocubes (1/6 of the total surface area) and independent of the edge length, the RI sensitivity drop should consequently also be constant (16.7%) according to the effective medium model. Results from the FDTD simulations show that the reduction is not exactly constant but depends on the size of the nanocubes, which could be explained by the near-field EM redistributions, as previously discussed. The deviations between the FDTD calculations and the effective medium model are, however, rather small, and the largest difference is ∼6%, seen for nanocubes with an edge length of 60 nm. For particles with an edge length larger than 60 nm, dephasing and multiple plasmon mode excitations make the calculations more difficult (Figure S2, Supporting Information), making it hard to theoretically determine the RI sensitivity. The small difference between the two models suggests that the effective medium approximation gives a rather accurate prediction of the RI sensitivity drop for a quite large range of nanoparticle sizes. However, the fractional contact area is not as easily estimated for heterogeneous nanoparticle populations and anisotropic nanoparticles, where various surface immobilization orientations are possible, making it much more difficult to estimate the substrate effect on the RI sensitivity using the effective medium model.

To examine if the substrate influence on the RI sensitivity could be minimized using a different surface immobilization strategy, we functionalized glass surfaces with PE layers as an optional strategy for immobilization of the silver nanoparticles. A layer-by-layer assembly of PEs is a common method to immobilize negatively charged nanoparticles mainly exploiting the electrostatic attraction between the topmost positively charged PE layer and the negatively charged nanoparticles.[23] We first coated glass substrates with PEI, followed by various numbers (n) of layers of PSS and PAH) with the positively charged PAH as the top layer. The RI sensitivity was investigated for the different silver nanoparticles immobilized on PE layers with n = 5, 9, 13, and 17 layers in total to examine whether the distance to the glass affected the sensitivity. Figure 5 shows RI sensitivity plots obtained for nanospheres, nanocubes, and nanoplates, respectively, immobilized on PE layers. No influence the RI sensitivity and only very small differences in sensitivity were observed with increasing number of PE layers. The RI sensitivity obtained for particles attached to PEs was slightly higher than that on surfaces modified with APTES: 145, 137, and 208 nm/RIU on average for nanospheres, nanocubes, and nanoplates, respectively, on PE layers compared with 140, 124, and 200 nm/RIU on APTES. This marginally higher sensitivity is probably an effect of the slightly lower RI of a PE film ($n \approx 1.46$) compared with that of borosilicate glass ($n \approx 1.52$). It is, however, possible that by increasing the polymer thickness further or using substrates composed solely of a polymeric material the substrate effect could be further reduced.

CONCLUSIONS

In summary, we have presented a detailed investigation of the effect of immobilization on the bulk RI sensitivity for three different geometries of silver nanoparticles (spheres, cubes, and plates). Both experimental and theoretical results show that the RI sensitivity was reduced when particles were attached to a solid support and that the quantity of this decrease was directly proportional to the fraction of the surface area in contact with the substrate. Nanospheres show essentially no reduction in the RI sensitivity upon immobilization, while nanocubes and nanoplates, which have a larger surface area in contact with the substrate, show a significant decrease in sensitivity. Thus, nanoparticles with sharp corners and edges exposed to the ambient media with limited or no contact with a supporting substrate would consequently exhibit a higher RI sensitivity

dx.doi.org/10.1021/jp5084086 | J. Phys. Chem. C 2014, 118, 24680−24687

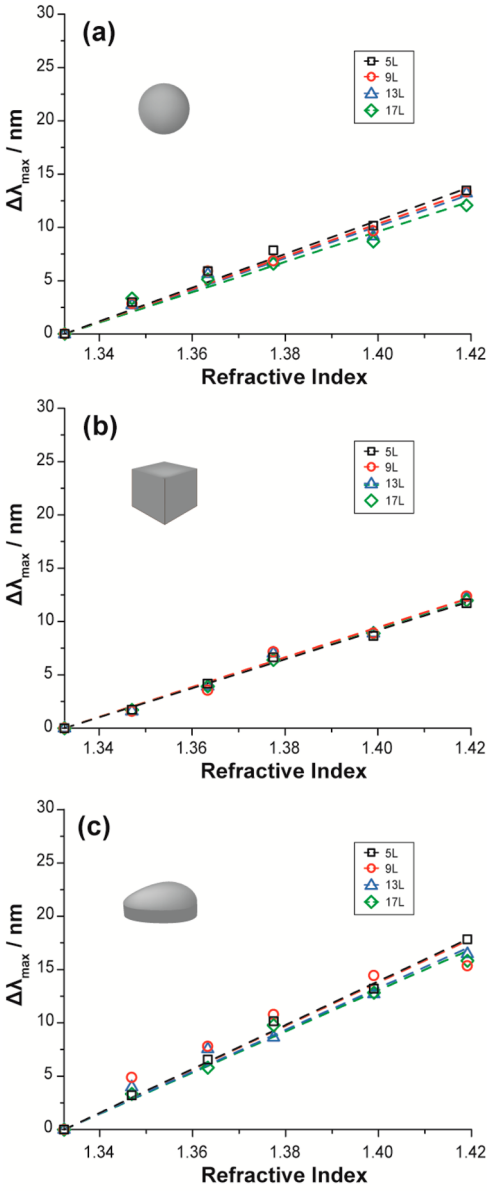

Figure 5. Refractive index sensitivity plots of silver nanospheres (a), nanocubes (b), and nanoplates (c) immobilized on different number of layers (n = 5, 9, 13, and 17) of polyelectrolytes.

than particles with a large area in contact with the substrate. The results presented here emphasize the importance of selecting appropriate nanostructures when constructing nanoplasmonic sensing devices to minimize the substrate effect and maximize the sensing performance.

■ ASSOCIATED CONTENT

Supporting Information

TEM images and size distribution data for the silver nanoparticles and theoretical extinction spectra generated by FDTD simulations for silver nanocubes. This material is available free of charge via the Internet at http://pubs.acs.org.

■ AUTHOR INFORMATION

Corresponding Author

*E-mail: daniel.aili@liu.se.

Author Contributions

The manuscript was written through contributions of all authors. All authors have given approval to the final version of the manuscript.

Notes

The authors declare no competing financial interest.

■ ACKNOWLEDGMENTS

Anders Elfwing is acknowledged for his assistance with the SEM measurements. D.A. and E.M. gratefully acknowledge financial support from the Swedish Research Council (VR) and the Swedish Foundation for Strategic Research (SSF). During this study, E.M. was enrolled in the graduate school Forum Scientium. B.S. and M.A.O acknowledge the financial support of the Spanish project MAT2011-12645-E.

■ REFERENCES

(1) Anker, J. N.; Hall, W. P.; Lyandres, O.; Shah, N. C.; Zhao, J.; Van Duyne, R. P. Biosensing with Plasmonic Nanosensors. *Nat. Mater.* **2008**, *7*, 442−453.

(2) Sepulveda, B.; Angelome, P. C.; Lechuga, L. M.; Liz-Marzan, L. M. LSPR-based nanobiosensors. *Nano Today* **2009**, *4*, 244−251.

(3) Petryayeva, E.; Krull, U. J. Localized surface plasmon resonance: Nanostructures, bioassays and biosensing-A review. *Anal. Chim. Acta* **2011**, *706*, 8−24.

(4) Estevez, M. C.; Otte, M. A.; Sepulveda, B.; Lechuga, L. M. Trends and challenges of refractometric nanoplasmonic biosensors: A review. *Anal. Chim. Acta* **2014**, *806*, 55−73.

(5) Stewart, M. E.; Anderton, C. R.; Thompson, L. B.; Maria, J.; Gray, S. K.; Rogers, J. A.; Nuzzo, R. G. Nanostructured plasmonic sensors. *Chem. Rev.* **2008**, *108*, 494−521.

(6) Yguerabide, J.; Yguerabide, E. E. Light-scattering submicroscopic particles as highly fluorescent analogs and their use as tracer labels in clinical and biological applications - I. Theory. *Anal. Biochem.* **1998**, *262*, 137−156.

(7) Miller, M. M.; Lazarides, A. A. Sensitivity of metal nanoparticle surface plasmon resonance to the dielectric environment. *J. Phys. Chem. B* **2005**, *109*, 21556−21565.

(8) Kelly, K. L.; Coronado, E.; Zhao, L. L.; Schatz, G. C. The optical properties of metal nanoparticles: The influence of size, shape, and dielectric environment. *J. Phys. Chem. B* **2003**, *107*, 668−677.

(9) Lee, K. S.; El-Sayed, M. A. Gold and silver nanoparticles in sensing and imaging: Sensitivity of plasmon response to size, shape, and metal composition. *J. Phys. Chem. B* **2006**, *110*, 19220−19225.

(10) Liz-Marzan, L. M. Tailoring surface plasmons through the morphology and assembly of metal nanoparticles. *Langmuir* **2006**, *22*, 32−41.

(11) Jones, M. R.; Osberg, K. D.; Macfarlane, R. J.; Langille, M. R.; Mirkin, C. A. Templated techniques for the synthesis and assembly of plasmonic nanostructures. *Chem. Rev.* **2011**, *111*, 3736−3827.

(12) Xia, Y. N.; Xiong, Y. J.; Lim, B.; Skrabalak, S. E. Shape-controlled synthesis of metal nanocrystals: simple chemistry meets complex physics? *Angew. Chem., Int. Ed.* **2009**, *48*, 60−103.

(13) Sun, Y. G.; Xia, Y. N. Shape-controlled synthesis of gold and silver nanoparticles. *Science* **2002**, *298*, 2176−2179.

(14) Svedendahl, M.; Chen, S.; Dmitriev, A.; Kall, M. Refractometric sensing using propagating versus localized surface plasmons: a direct comparison. *Nano Lett.* **2009**, *9*, 4428−4433.

(15) Martinsson, E.; Shahjamali, M. M.; Enander, K.; Boey, F.; Xue, C.; Aili, D.; Liedberg, B. Local refractive index sensing based on edge gold-coated silver nanoprisms. *J. Phys. Chem. C* **2013**, *117*, 23148−23154.

(16) Otte, M. A.; Sepulveda, B.; Ni, W. H.; Juste, J. P.; Liz-Marzan, L. M.; Lechuga, L. M. Identification of the optimal spectral region for plasmonic and nanoplasmonic sensing. *ACS Nano* **2010**, *4*, 349−357.

(17) Xue, C.; Li, Z.; Mirkin, C. A. Large-scale assembly of single-crystal silver nanoprism monolayers. *Small* **2005**, *1*, 513−516.

(18) Zhang, X. Y.; Hu, A. M.; Zhang, T.; Lei, W.; Xue, X. J.; Zhou, Y. H.; Duley, W. W. Self-assembly of large-scale and ultrathin silver nanoplate films with tunable plasmon resonance properties. *ACS Nano* **2011**, *5*, 9082−9092.
(19) Dahl, J. A.; Maddux, B. L. S.; Hutchison, J. E. Toward greener nanosynthesis. *Chem. Rev.* **2007**, *107*, 2228−2269.
(20) Aili, D.; Gryko, P.; Sepulveda, B.; Dick, J. A. G.; Kirby, N.; Heenan, R.; Baltzer, L.; Liedberg, B.; Ryan, M. P.; Stevens, M. M. Polypeptide folding-mediated tuning of the optical and structural properties of gold nanoparticle assemblies. *Nano Lett.* **2011**, *11*, 5564−5573.
(21) Scarpettini, A. F.; Bragas, A. V. Coverage and aggregation of gold nanoparticles on silanized Glasses. *Langmuir* **2010**, *26*, 15948−15953.
(22) Aureau, D.; Varin, Y.; Roodenko, K.; Seitz, O.; Pluchery, O.; Chabal, Y. J. Controlled deposition of gold nanoparticles on well-defined organic mono layer grafted on silicon surfaces. *J. Phys. Chem. C* **2010**, *114*, 14180−14186.
(23) Nooney, R. I.; Stranik, O.; McDonagh, C.; MacCraith, B. D. Optimization of plasmonic enhancement of fluorescence on plastic substrates. *Langmuir* **2008**, *24*, 11261−11267.
(24) Knight, M. W.; Wu, Y. P.; Lassiter, J. B.; Nordlander, P.; Halas, N. J. Substrates matter: influence of an adjacent dielectric on an individual plasmonic nanoparticle. *Nano Lett.* **2009**, *9*, 2188−2192.
(25) Chen, H. J.; Ming, T.; Zhang, S. R.; Jin, Z.; Yang, B. C.; Wang, J. F. Effect of the dielectric properties of substrates on the scattering patterns of gold nanorods. *ACS Nano* **2011**, *5*, 4865−4877.
(26) Valamanesh, M.; Borensztein, Y.; Langlois, C.; Lacaze, E. Substrate effect on the plasmon resonance of supported flat silver nanoparticles. *J. Phys. Chem. C* **2011**, *115*, 2914−2922.
(27) Novo, C.; Funston, A. M.; Pastoriza-Santos, I.; Liz-Marzan, L. M.; Mulvaney, P. Influence of the medium refractive index on the optical properties of single gold triangular prisms on a substrate. *J. Phys. Chem. C* **2008**, *112*, 3−7.
(28) Dmitriev, A.; Hagglund, C.; Chen, S.; Fredriksson, H.; Pakizeh, T.; Kall, M.; Sutherland, D. S. Enhanced nanoplasmonic optical sensors with reduced substrate effect. *Nano Lett.* **2008**, *8*, 3893−3898.
(29) Otte, M. A.; Estevez, M. C.; Carrascosa, L. G.; Gonzalez-Guerrero, A. B.; Lechuga, L. M.; Sepulveda, B. Improved biosensing capability with novel suspended nanodisks. *J. Phys. Chem. C* **2011**, *115*, 5344−5351.
(30) Brian, B.; Sepulveda, B.; Alaverdyan, Y.; Lechuga, L. M.; Kall, M. Sensitivity enhancement of nanoplasmonic sensors in low refractive index substrates. *Opt. Express* **2009**, *17*, 2015−2023.
(31) Zhang, S. P.; Bao, K.; Halas, N. J.; Xu, H. X.; Nordlander, P. Substrate-induced fano resonances of a plasmonic: nanocube: a route to increased-sensitivity localized surface plasmon resonance sensors revealed. *Nano Lett.* **2011**, *11*, 1657−1663.
(32) Sherry, L. J.; Chang, S. H.; Schatz, G. C.; Van Duyne, R. P.; Wiley, B. J.; Xia, Y. N. Localized surface plasmon resonance spectroscopy of single silver nanocubes. *Nano Lett.* **2005**, *5*, 2034−2038.
(33) Ringe, E.; McMahon, J. M.; Sohn, K.; Cobley, C.; Xia, Y. N.; Huang, J. X.; Schatz, G. C.; Marks, L. D.; Van Duyne, R. P. Unraveling the Effects of Size, Composition, and Substrate on the Localized Surface Plasmon Resonance Frequencies of Gold and Silver Nanocubes: A Systematic Single-Particle Approach. *J. Phys. Chem. C* **2010**, *114*, 12511−12516.
(34) Hagemann, H.-J.; Gudat, W.; Kunz, C. Optical constants from the far infrared to the X-ray region: Mg, Al, Cu, Ag, Au, Bi, C, and Al_2O_3. *J. Opt. Soc. Am.* **1975**, *65*, 742−744.
(35) Zhang, Q. A.; Li, W. Y.; Wen, L. P.; Chen, J. Y.; Xia, Y. N. Facile synthesis of Ag nanocubes of 30 to 70 nm in edge length with CF3COOAg as a precursor. *Chem.—Eur. J.* **2010**, *16*, 10234−10239.
(36) Shahjamali, M. M.; Bosman, M.; Cao, S. W.; Huang, X.; Saadat, S.; Martinsson, E.; Aili, D.; Tay, Y. Y.; Liedberg, B.; Loo, S. C. J.; Zhang, H.; Boey, F.; Xue, C. Gold coating of silver nanoprisms. *Adv. Funct. Mater.* **2012**, *22*, 849−854.
(37) Shahjamali, M. M.; Bosman, M.; Cao, S. W.; Huang, X.; Cao, X. H.; Zhang, H.; Pramana, S. S.; Xue, C. Surfactant-free sub-2 nm ultrathin triangular gold nanoframes. *Small* **2013**, *9*, 2880−2886.
(38) Otte, M. A.; Sepulveda, B. Figures of Merit for Refractometric LSPR Biosensing. In *Nanoplasmonic Sensors*; Dmitriev, A., Ed.; Springer: New York, 2012.